# MODELING AND CONTROL OF SATELLITE FORMATIONS IN HIGH ECCENTRICITY ORBITS[1]

**Prasenjit Sengupta[2], Srinivas R. Vadali[3] and Kyle T. Alfriend[4]**

An analytical method has been developed to propagate the relative motion between two satellites in highly elliptic orbits. The method is kinematically exact. It maintains a high degree of accuracy even in the presence of $J_2$ perturbations arising from the non-spherical nature of the Earth. The true anomaly of the reference satellite is treated as the independent variable, instead of time. The relative orbit kinematics is studied by using a projection onto a unit sphere. This procedure allows the relative position variables to be treated as angles that depend on the orbital element differences. Mean orbital elements are used for orbit propagation and expansions involving the powers of eccentricity are not utilized. The final results are obtained by converting the mean elements into osculating elements using Brouwer's theory. The effect of adding short-period corrections to the mean elements is also studied. The developed analytical model and numerical optimization are employed to perform reconfiguration maneuvers by application of impulsive thrust.

## Introduction

The study of relative motion of satellites in orbits about the Earth or in deep space is of great current interest, primarily due to applications in space-based interferometry and

[1]Presented as paper AAS 03-277 at the John L. Junkins Astrodynamics Symposium in College Station, Texas, May 23-24,2003.

[2]Graduate Student, Department of Aerospace Engineering, Texas A&M University, College Station, TX 77843-3141, prasenjit@tamu.edu, Student Member AAS.

[3]Stewart & Stevenson-I Professor, Department of Aerospace Engineering, Texas A&M University, College Station, TX 77843-3141, svadali@aero.tamu.edu, Member AAS.

[4]Wisenbaker II Professor, Department of Aerospace Engineering, Texas A&M University, College Station, TX 77843-3141, alfriend@aero.tamu.edu, Fellow AAS.

distributed multi-aperture systems. Satellite formations are characterized by the shapes of the relative orbits between the satellites as well as the volume of the polyhedron obtained by treating each satellite as a vertex point. For example, circular and projected circular relative orbits have been proposed for a number of planned missions. Obtaining bounded relative motion with minimal use of propulsive fuel is a key to the success of any such mission. When the objective is to study the relative motion dynamics of two or more satellites, one of the satellites is generally considered as the reference satellite or the Chief. The other satellites are designated the Deputies.

There exist various models for describing the relative motion of satellites. The Hill-Clohessy-Wiltshire (HCW) equations [1] model relative motion dynamics under three assumptions: 1) Circular Chief orbit, 2) Spherical Earth and 3) Linearization of the differential gravitational acceleration. These equations provide a convenient platform for designing a preliminary relative orbit geometry. However, this description is no longer valid once any one or more of the three mentioned assumptions are violated. The HCW initial conditions can be corrected to produce bounded relative motion for such cases by accommodating the perturbations due to second-order nonlinearities in the differential gravitational attraction and the eccentricity of the Chief's orbit [2]. The $J_2$ perturbation associated with the aspherical Earth causes the orbital elements that characterize an orbit to change over time, resulting in drift and unbounded relative motion. This drift can be virtually eliminated for small orbit element differences using the concept of $J_2$-invariant relative orbits [3]. However, $J_2$-invariant relative orbits may not be attractive for many missions due to the large relative orbit sizes obtained. Hence, a rate-matching constraint has been developed [4] to keep the along-track motion bounded. The out-of-plane motion can be controlled by application of

thrust, as required.

Analytical expressions for propagating relative motion under the influence of $J_2$ have been developed by several authors. Gim et al. [5] provide a state transition matrix for the solution of the linearized relative motion problem using curvilinear coordinates. Schaub [6] presents analytical expressions for propagating the linearized orbital element differences using the true anomaly as the independent variable. His approach does not require the solution of Kepler's equation at each required value of the true anomaly. Time-explicit solutions have been developed by Sabol et al. [7] using eccentricity expansions. This approach is valid for small eccentricities. A kinematically-exact description using the unit sphere approach [8] has also been developed. In this approach, the relative motion problem is studied by projecting the motion of the satellites onto a unit sphere. This is achieved by normalizing the position vector of each satellite with respect to its radius. This process allows one to study the relative motion using spherical trigonometry. The original unit sphere approach also uses eccentricity expansions for the radial distance and argument of latitude in order to obtain time-explicit expressions. These eccentricity expansions are not uniformly convergent for high eccentricities. Even for moderate eccentricities, the number of terms required for convergence cannot be determined *a priori*. In such cases it becomes necessary to solve Kepler's equation for each satellite in the formation at every solution point. In this paper, the true anomaly of the Chief is used as the independent variable, rather than time. It will be shown that even for high eccentricity relative orbits and large relative orbit radii, the unit sphere approach produces accurate results. Kepler's equation has to be solved, but only for the Deputies.

The formation has to be controlled for establishment of the relative orbit, orbit recon-

figuration, or orbit maintenance, in the presence of $J_2$ and drag perturbations. If velocity increments (impulsive thrust assumption) are used, then Gauss' equations can be used to find the changes in orbital elements arising due to these increments. The analysis in this paper assumes that the Chief is uncontrolled and impulses are used to control a Deputy. The analytical solution developed in this paper is used to propagate the orbits of the satellites during the coasting phases. The optimal magnitude and directions of the impulses, as well as the optimal time instants (true anomaly) of thrust application are evaluated using numerical optimization techniques. To maintain computational accuracy for highly eccentric orbits, the values of the true anomaly of the Chief at points of thrust application are optimized, instead of the times of thrust application. The validity of the results are verified by using the data obtained from the optimization process in a numerical integration-based simulation.

## The Unit Sphere Approach

### Frames of Reference

The analysis in this paper uses the frames of reference shown in Fig. 1. The Earth-Centered Inertial (ECI) frame, denoted by $X$-$Y$-$Z$ has axes along the unit vectors $\mathbf{i}_X$, $\mathbf{i}_Y$ and $\mathbf{i}_Z$ as shown. The Local-Vertical-Local-Horizontal (LVLH) frame, denoted by $r$-$\theta$-$h$ for each satellite, has its axes along the unit vectors $\mathbf{i}_r$, $\mathbf{i}_\theta$ and $\mathbf{i}_h$. The unit vector $\mathbf{i}_r$, lies along the line joining the center of the Earth to the satellite, and $\mathbf{i}_h$ is the vector normal to the plane defined by the position and velocity vectors of the satellite. The third vector $\mathbf{i}_\theta$, that is mutually perpendicular to $\mathbf{i}_r$ and $\mathbf{i}_h$, completes the set. Each satellite has its own associated LVLH frame, and any vector in the ECI frame can be transformed into the LVLH frame

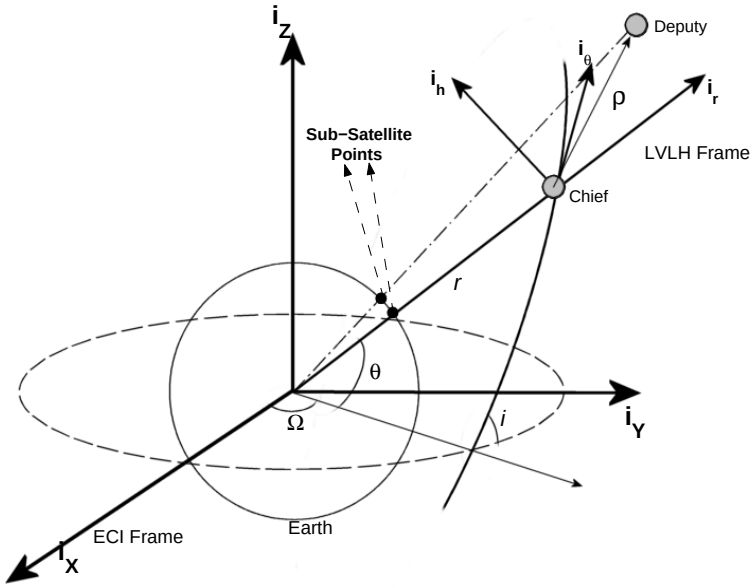


**Figure 1** Frames and Sub-Satellite Points

through the direction cosine matrix. The direction cosine matrix is characterized by an Euler 3-1-3 rotation [9] using the right ascension $\Omega$, inclination $i$, and argument of latitude $\theta$. For any orbit, $\theta = \omega + f$, where $\omega$ is the argument of perigee and $f$ is the true anomaly.

## Unit Sphere Model

The relative motion between two satellites can be analytically obtained by projecting the positions of the Chief and Deputy to their sub-satellite points on the unit sphere, which are calculated by normalizing their positions with respect to their radial distances. If $\mathbf{C}_C$ and $\mathbf{C}_D$ are the direction cosine matrices associated with the LVLH frames of the Chief and the Deputy, respectively, then the relative position of the Deputy with respect to the Chief,

on the unit sphere, is given by

$$\left\{ \begin{array}{c} \Delta x \\ \Delta y \\ \Delta z \end{array} \right\} = \left[ \mathbf{C}_C \mathbf{C}_D^T - \mathbf{I} \right] \left\{ \begin{array}{c} 1 \\ 0 \\ 0 \end{array} \right\} \tag{1}$$

The matrix $\mathbf{C}_C \mathbf{C}_D^T$ is the direction cosine matrix that transforms a vector in the Deputy's LVLH frame into the Chief's LVLH frame. Since $\mathbf{C}_C \equiv \mathbf{C}_C(\Omega_C, i_C, \theta_C)$ and $\mathbf{C}_D \equiv \mathbf{C}_D(\Omega_D, i_D, \theta_D)$, the relative position requires the determination of these angles. The true relative position in the LVLH frame of the Chief is then given by the inverse relations

$$\begin{aligned} \delta x &= r_D(1 + \Delta x) - r_C \\ \delta y &= r_D \Delta y \\ \delta z &= r_D \Delta z \end{aligned} \tag{2}$$

Equation (1) can be expanded [8] into expressions that contain the elemental angle differences between the Deputy and Chief (viz. $\Delta\Omega$, $\Delta i$ and $\Delta\theta$):

$$\begin{aligned} \Delta x &= -1 + c_{i_C/2}^2 c_{i_D/2}^2 c_{(\Delta\theta+\Delta\Omega)} + s_{i_C/2}^2 s_{i_D/2}^2 c_{(\Delta\theta-\Delta\Omega)} \\ &\quad + s_{i_C/2}^2 c_{i_D/2}^2 c_{(2\theta_C+\Delta\theta+\Delta\Omega)} + c_{i_C/2}^2 s_{i_D/2}^2 c_{(2\theta_C+\Delta\theta-\Delta\Omega)} \\ &\quad + 1/2 s_{i_C} s_{i_D} \left[ c_{\Delta\theta} - c_{(2\theta_C+\Delta\theta)} \right] \\ \Delta y &= c_{i_C/2}^2 c_{i_D/2}^2 s_{(\Delta\theta+\Delta\Omega)} + s_{i_C/2}^2 s_{i_D/2}^2 s_{(\Delta\theta-\Delta\Omega)} \\ &\quad - s_{i_C/2}^2 c_{i_D/2}^2 s_{(2\theta_C+\Delta\theta+\Delta\Omega)} - c_{i_C/2}^2 s_{i_D/2}^2 c_{(2\theta_C+\Delta\theta-\Delta\Omega)} \end{aligned} \tag{3}$$

$$+1/2 s_{i_C} s_{i_D} \left[ s_{\Delta\theta} + s_{(2\theta_C + \Delta\theta)} \right]$$

$$\Delta z = -s_{i_C} s_{\Delta\Omega} c_{\theta_D} - \left[ s_{i_C} c_{i_D} c_{\Delta\Omega} - c_{i_C} s_{i_D} \right] s_{\theta_D}$$

where $s$ and $c$ with the corresponding subscripts, denote the sine and cosine functions with the subscripts as arguments, respectively. Equations (3) depend on two angles of the Chief - $i_C$ and $\theta_C$, and the angle differences between the Deputy and Chief - $\Delta\Omega$, $\Delta i$ and $\Delta\theta$. Since the $J_2$ perturbations are symmetric about the $Z$ axis of the Earth, $\Omega_C$ does not appear in the equations of relative motion.

### True Relative Position for Low Eccentricity Orbits

The Euler angle description, with the angles propagated with mean rates, can be used to find the relative position on the unit sphere. To find the true relative position, $r$ and $\theta$ have to be determined. For low eccentricities, the following eccentricity expansions for $r$ and $\theta$ may be used to a reasonable degree of accuracy [10]:

$$r \approx a \left[ 1 - e \cos M - 0.5 e^2 (\cos 2M - 1) \right] \tag{4}$$

$$\theta \approx \omega + M + 2e \sin M + 1.25 e^2 \sin 2M \tag{5}$$

In the presence of $J_2$, the angles $\Omega$, $\omega$ and $M$ can be obtained using mean elements containing only secular rates, by the following equations

$$\begin{aligned} \Omega(t) &= \Omega(0) + \dot{\Omega} t \\ \omega(t) &= \omega(0) + \dot{\omega} t \\ M(t) &= M(0) + \dot{M} t \end{aligned} \tag{6}$$

where,

$$\begin{aligned}
\dot{\Omega} &= -\frac{3}{2} n J_2 \left(\frac{R_e}{p}\right)^2 \cos i \\
\dot{\omega} &= \frac{3}{4} n J_2 \left(\frac{R_e}{p}\right)^2 (5\cos^2 i - 1) \\
\dot{M} &= n\left[1 + \frac{3}{4}\sqrt{1-e^2} J_2 \left(\frac{R_e}{p}\right)^2 (3\cos^2 i - 1)\right]
\end{aligned} \tag{7}$$

From equations (2)-(7), the true relative position can be found analytically.

## Initial Conditions for Relative Motion

For reference orbits with near-zero mean eccentricity much attention has been focused on a specific relative orbit, whose projection on the local horizontal plane ($\theta$-$h$) is a circle. This relative orbit is characterized by two quantities - its radius $\rho$ and initial phase angle $\alpha_0$. From the period-matching condition in the presence of $J_2$ perturbations [4] and the geometry of the relative orbit, the elemental differences between Deputy and Chief can be computed from:

$$\begin{aligned}
\delta i &= \frac{\rho}{a_C} \cos\alpha_0 \\
\delta e &= -\frac{\rho}{2a_C} \left[\sin(\omega_C + \alpha_0) + 2e_C \sin(M_{C_0} + \omega_C + \alpha_0)\right] \\
\delta a &= \frac{1}{2} J_2 \left(\frac{R_e^2}{a_C}\right) \frac{\left(3\sqrt{1-e_C^2}+4\right)}{(1-e_C^2)^2} \left[-(1-3\cos^2 i_C)\frac{e_C}{1-e_C^2}\delta e - \sin 2i_C \delta i\right] \\
\delta\Omega &= -\frac{\rho}{a_C \sin i_C} \sin\alpha_0 \\
\delta\omega &= \frac{\rho}{a_C}\left[\frac{\sin\alpha_0}{\tan i_C} - \frac{1}{2e_C}\cos(\omega_C + \alpha_0)\right] \\
\delta M &= \frac{\rho}{2a_C e_C} \cos(\omega_C + \alpha_0)
\end{aligned} \tag{8}$$

Though the above formulae have been derived from a linearized theory, they yield remarkably regular results for large formations also. For low eccentricities, the second term for $\delta e$ is very small when compared with the first, and can be neglected. For higher eccentricities, the shape of the relative orbit tends to degenerate and no longer projects into a circle. However, this paper will continue to characterize such non-circular orbits by using $\rho$ and $\alpha_0$. Equations (8) have a singularity associated with a circular Chief's orbit, i.e., $e_C = 0$, though they can be used to obtain orbital elemental differences for cases where the Chief's orbit has low eccentricities. Reference 11 uses non-singular elements; this allows the computation of the elements of the Deputy when the Chief is in a circular orbit.

## Modified Method for Orbits of High Eccentricity

The expressions (4) and (5) are only valid for reference orbits of low eccentricity. As the eccentricity increases, additional terms need to be included in the series. Unfortunately, convergence is not guaranteed in this case, and after a limit, the series expansion does not converge at all. Since $\theta = \omega + f$, and $r = a(1 - e\cos E)$ (with eccentric anomaly $E$), Kepler's equation needs to be solved for $E$ and $f$ needs to be calculated from $E$:

$$M = E - e\sin E, \quad \cos E = \frac{e + \cos f}{1 + e\cos f} \tag{9}$$

In order to avoid solving Kepler's equation iteratively for the Chief, one may use $f_C$ as the independent variable. Subsequently, from equation (9), the time corresponding to the mean anomaly can be obtained as follows:

$$t = t_0 + \frac{M(t) - M(t_0)}{\dot{M}} \tag{10}$$

With the time obtained from equation (10), equations (6) can be used to calculate the remaining 5 angles - $\Omega_C$, $\omega_C$, $\Omega_D$, $\omega_D$ and $M_D$.

The advantage of this method over the method of stepping through time is immediately apparent when one considers positions on highly eccentric orbits that are near the perigee. Quantities near the perigee change very fast, and one would require time steps that are much smaller near the perigee than near the apogee. This is automatically taken care of by stepping through $f_C$. Additionally, it will be shown that for high-eccentricity orbits, if the formation is established at perigee ($M_0 = 0°$), small errors in initial conditions can cause significant errors between the results of the analytical propagation and the integration of the 12th-order ECI system (truth model), when compared to the errors obtained when the orbit is established near the apogee ($M_0 = 180°$).

### Osculating Elements in the Unit Sphere Model

There has been extensive study on the motion of a single satellite in the absence of drag, but with the effects of an oblate Earth included. Brouwer [12] developed a transformation between mean and osculating elements through the use of perturbation analysis of the Hamiltonian formed by the Delauney orbital elements. Kozai [13] expanded the gravitational potential including that due to $J_2$ into four classes - first-order secular, second-order secular, short period (dependent on the true anomaly) and long-period (dependent on the argument of perigee). The first-order secular terms are already taken into account in the mean rates for $\Omega$, $\omega$ and $M$, shown in equations (7). The semimajor axis $a$, eccentricity $e$, and inclination $i$, do not show secular growth. The short period corrections from Kozai and Brouwer are identical [14], and long period corrections are not significant in the analysis

presented in this paper. The unit sphere approach is tested by using corrected elements from Brouwer's theory that account for short as well as long period variations. Unless explicitly stated, all the simulation results presented in this paper were obtained using the transformation of mean elements into osculating elements.

## Impulse Control

In this section optimal two-impulse maneuvers are considered for reconfiguring a formation characterized by relative radius $\rho_i$ and initial phase angle $\alpha_{0_i}$, to one characterized by $\rho_f$ and $\alpha_{0_f}$. In Vaddi [15], sub-optimal velocity impulses were obtained to establish and reconfigure a formation. In this paper optimal two-impulse maneuvers for reconfiguration of large formations, in the presence of $J_2$ and high-eccentricity of the Chief are obtained using numerical optimization.

### Gauss' Equations

Gauss' equations [10] relate the control accelerations to the corresponding changes in orbital elements. Given a control acceleration $\mathbf{u} = \{u_X \quad u_Y \quad u_Z\}^T$, the rates of change of orbital elements are given by

$$\frac{d\mathbf{e}}{dt} = \mathbf{f}(\mathbf{e}, \mathbf{u}) \tag{11}$$

where $\mathbf{e} = \{a \quad e \quad i \quad \Omega \quad \omega \quad M\}^T$. If the controls are applied in the form of velocity impulses then $\mathbf{u}dt \approx \Delta\mathbf{v} = \{v_X \quad v_Y \quad v_Z\}^T$ and $d\mathbf{e} \approx \Delta\mathbf{e}$. In such cases, the changes in

the orbital elements are given by the following relationship:

$$\Delta\mathbf{e} \quad = \quad \mathbf{G}(\mathbf{e})\Delta\mathbf{v}$$

where,

$$\mathbf{G} \quad = \quad \begin{bmatrix} \frac{2a^2}{h} e \sin f & \frac{2a^2}{h}\frac{p}{r} & 0 \\ \frac{p \sin f}{h} & \frac{(p+r)\cos f + re}{h} & 0 \\ 0 & 0 & \frac{r\cos\theta}{h} \\ 0 & 0 & \frac{r\sin\theta}{h\sin i} \\ -\frac{p\cos f}{he} & \frac{(p+r)\sin f}{he} & -\frac{r\sin\theta\cos i}{h\sin i} \\ \frac{\eta}{he}(p\cos f - 2re) & -\frac{\eta}{he}(p+r)\sin f & 0 \end{bmatrix} \tag{12}$$

with $h = \sqrt{\mu p}$, $\eta = \sqrt{1-e^2}$, $r = p/(1 + e\cos f)$ and $p = a(1-e^2)$.

## Formulation of an Optimal Control Problem (OCP)

Each velocity impulse has three components. It is possible to control two orbital elements with a single impulse which is suitably placed. For example, if it is desired to change the angles of inclination and right ascension, it is evident from equation (12) that by choosing an appropriate value of $\theta$, both can by changed simultaneously by the same normal component of velocity impulse. However, it is not possible to change all the six orbital elements by a single velocity impulse. In the above example, the change in the remaining four orbital elements by two in-plane impulse components would lead to four equations in two variables. Therefore, at least two impulses are required to obtain the six desired orbital element changes. Considering the general case of $N$ impulses, the number of variables to optimize

are $3N + N = 4N$ which correspond to the three components per velocity impulse, and $N$ optimal positions for impulse application. Keeping in mind the problems associated with formations where the Chief's orbit has high eccentricity, the true anomaly of the Chief is used as the independent variable instead of time. The cost function used is the sum of the magnitudes of the velocity increments, given by

$$J = \sum_{i=1}^{N} W_i |\Delta \mathbf{v}_i| \tag{13}$$

where $W_i$ is the weight associated with each impulse, and $|\cdot|$ denotes the vector norm.

## Algorithm

Initial guesses are made for the components of the the $N$ velocity impulses and $N$ true anomalies at which they are applied. The initial conditions provided are the relative orbit parameters $(\rho_i, \alpha_{0_i})$. Since the initial conditions of the Chief are known, the initial conditions for the Deputy are obtained from equations (8). The motions of both the satellites (Chief and Deputy) are propagated using the mean element formulation with the rates given by equations (7). Steps are taken in $f_C$ until the first true anomaly value of firing is reached. The elements are updated using the $\mathbf{G}$ matrix in equation (12). The process is repeated until all the $N$ impulses are applied. Let the elements of the Deputy after the last impulse be $\mathbf{e}_D(f_N)$. Since the final conditions are specified in the form of $(\rho_f, \alpha_{0_f})$, the desired final value of the elements of the Deputy are

$$\mathbf{e}_{D_f} = \mathbf{e}_C(f_N) + \delta\mathbf{e}(\rho_f, \alpha_{0_f})$$

Thus, 6 non-linear constraints to the OCP are obtained, given by

$$|\mathbf{e}_D(f_N) - \mathbf{e}_C(f_N) - \delta\mathbf{e}(\rho_f, \alpha_{0_f})| = \mathbf{0} \tag{14}$$

Equations (13) and (14) are used with the FORTRAN package NPOPT [16] to solve the OCP numerically.

Though the velocity impulses are obtained from a mean element analysis, they are simulated by the integration of the 12th order nonlinear ECI system of equations. The equations for inertial position $\mathbf{r}_D$ and velocity $\mathbf{v}_D$ are propagated until an impulse time $t_i$, $i = 1 \ldots N$. At this point the orbital elements $\mathbf{e}_D(t_i)$ are obtained from $\mathbf{r}_D(t_i)$ and $\mathbf{v}_D(t_i)$. Since these are osculating elements, they need to be converted to mean elements for consistency with the method used to obtain the impulses. The inertial position and velocity corresponding to the mean elements are obtained, and the velocity increment $\boldsymbol{\Delta}\mathbf{v}_i$ is added to the mean inertial velocity. Inertial position does not change on application of a velocity impulse. The mean position and velocity after the impulse are converted to mean orbital elements and subsequently to osculating orbital elements. The osculating inertial position and velocity obtained from these orbital elements are used as initial conditions for the next stage of propagation, from $t_i$ to $t_{i+1}$. The process is repeated for each impulse.

## Numerical Simulations

The algorithms developed in this paper will be illustrated in this section for different cases.

## Comparison of the Results from the Modified Unit Sphere Approach and Numerical Integration

In Vadali [8], the accuracy of the unit sphere model has already been demonstrated for reference orbits of low eccentricity. Here, a high-eccentricity case is considered for a reference orbit that has an apogee of $12R_e$ and perigee distance of $1.2R_e$, where $R_e$ is the radius of the Earth. The inclination of the orbit is selected to be $50^\circ$. The initial mean elements of the Chief's orbit are:

$$\mathbf{e}_C = \{42095.7\text{km} \quad 0.8182 \quad 50^\circ \quad 0^\circ \quad 0^\circ \quad 180^\circ\}$$

The initial $M_C$ signifies the establishment of the orbit at apogee. The size of the relative orbit selected is given by $\rho = 20$km. Although the projected orbit is no longer circular, $\rho$ and $\alpha_0$ are still used to characterize the orbit. The initial mean orbital elements of the Deputy are obtained by using the equations (8). The initial conditions for the truth model are obtained by first converting the mean orbital elements of the Chief and Deputy to osculating orbital elements, and then converting osculating orbital elements to position and velocity.

Figure 2 shows the errors between the analytical and numerical orbit propagation schemes, in the presence of $J_2$ perturbations for $\alpha_0 = 0^\circ$. The figures on the left show the results obtained from the use of mean elements. The figures on the right show the results after applying the short-period and long-period corrections (osculating elements) from Brouwer's theory. Figure 3 shows these errors for $\alpha_0 = 90^\circ$. These results show that the unit sphere method in conjunction with osculating elements is highly accurate. The errors

obtained using the mean elements remain bounded over the period of 10 orbits. Figures 4 and 5 show the relative orbits obtained in each case.

Next, a large relative orbit with $\rho = 100$km is considered, with the mean elements of the Chief (excluding the initial value of the mean anomaly) chosen as $a_C = 12000$km, $e_C = 0.4$, $i_C = 50^\circ$, and $\Omega_C = \omega_C = 0^\circ$. Figures 6 and 7 show the errors between the analytical solution and integrated solution for $\alpha_0 = 0^\circ$ and $\alpha_0 = 90^\circ$, respectively, with the orbit established at perigee ($M_{C_0} = 0^\circ$), using the process outlined above. It is seen that by using osculating elements, the bias in the errors is considerably reduced along the $x$ and $z$ axes. Figures 8 and 9 show the errors for the same configurations, $\alpha_0 = 0^\circ$ and $\alpha_0 = 90^\circ$, but with the orbit established at apogee ($M = 180^\circ$). For the $\alpha_0 = 0^\circ$ case (Figure 8), the use of osculating elements reduces the errors to less than 1m, which is very accurate when the size of the relative orbit is considered. A reduction in the bias error in the radial and out-of-plane directions, is also seen in Fig. 9, corresponding to the $\alpha_0 = 90^\circ$ case. Comparing Figs. 6 and 8, and Figs. 7 and 9, the reduction in errors on establishing the formation at apogee is immediately apparent.

## Relative Orbit Reconfiguration

The reconfiguration of a formation is considered next. The formation is to be reconfigured from an initial relative orbit characterized by $(\rho_i, \alpha_{0_i})$ to one characterized by $(\rho_f, \alpha_{0_f})$. It is assumed that two impulses will be used, with the values of the true anomaly of the Chief for impulse application chosen for optimality. Two cases will be considered: one for a low eccentricity reference orbit with small $\rho$, and the other with a high eccentricity reference orbit with a larger $\rho$. In specific, the cases are as follows:

1. Low Eccentricity of the Chief's Orbit: in this case the mean elements of the Chief are

   $\mathbf{e}_C = \{7100\text{km} \quad 0.005 \quad 70^\circ \quad 0^\circ \quad 0^\circ \quad 0^\circ\}$.

2. High Eccentricity of the Chief's Orbit: the mean elements of the Chief are

   $\mathbf{e}_C = \{42095.70\text{km} \quad 0.8182 \quad 50^\circ \quad 0^\circ \quad 0^\circ \quad 11.76^\circ\}$

In the high eccentricity case, $M_{C_0} = 11.76^\circ$ corresponds to $f_{C_0} = 105^\circ$. This value is chosen arbitrarily and ensures that the formation is established far enough away from the perigee so that the errors from the analytical model are of the same order as those if the formation is established at apogee. This choice of $M_{C_0}$ also allows enough "room" for the first impulse to occur before the apogee is reached.

*Low Eccentricity Reconfiguration*: The reconfiguration from an initial formation of $\rho =$ 1km to one of $\rho = 2$km is considered, for two initial phase angles, $\alpha_0 = 0^\circ$ and $\alpha_0 = 90^\circ$. The variation of fuel cost with final phase angle is studied. Figure 10 shows the total impulse required (sum of magnitudes of velocity increments) using two impulses. It can be seen that the results for $\alpha_{0_i} = 90^\circ$ are almost exactly symmetrical to those for $\alpha_{0_i} = 0^\circ$. Furthermore, Reference 15 shows that if the initial $\alpha_0$ and final $\alpha_0$ are the same, then the total velocity impulse required is the same, irrespective of the value of $\alpha_0$.

The positions (true anomaly of Chief) and times of impulse application are obtained from the numerical optimization code using NPOPT, and are presented in Table 1.

It is observed that the tangential components of the impulses are negligible when compared with the radial and out-of-plane components. This is because there is negligible change in semi-major axis involved and radial impulses are used to change the eccentricity.

| $\alpha_{0_f}$ (deg) | Impulse 1 | | | | Impulse 2 | | | |
|---|---|---|---|---|---|---|---|---|
| | $f_{C_1}$ (deg) | $\Delta\mathbf{v}_1$ (m/s) | | | $f_{C_2}$ (deg) | $\Delta\mathbf{v}_2$ (m/s) | | |
| | | $\Delta v_{1_r}$ | $\Delta v_{1_\theta}$ | $\Delta v_{1_h}$ | | $\Delta v_{2_r}$ | $\Delta v_{2_\theta}$ | $\Delta v_{2_h}$ |
| 0 | 0.00 | 0.265 | -0.001 | 0.543 | 179.52 | -0.263 | 0.001 | -0.512 |
| 10 | 160.05 | -0.274 | 0.001 | -0.560 | 339.96 | 0.270 | -0.001 | 0.530 |
| 20 | 142.08 | -0.296 | 0.002 | -0.606 | 321.80 | 0.290 | -0.001 | 0.575 |
| 30 | 126.33 | -0.331 | 0.003 | -0.673 | 305.94 | 0.322 | -0.001 | 0.641 |
| 40 | 112.73 | -0.372 | 0.004 | -0.754 | 292.28 | 0.361 | -0.001 | 0.721 |
| 50 | 100.87 | -0.418 | 0.004 | -0.842 | 280.40 | 0.404 | -0.001 | 0.809 |
| 60 | 90.34 | -0.464 | 0.005 | -0.932 | 269.88 | 0.449 | -0.001 | 0.902 |
| 70 | 80.81 | -0.510 | 0.006 | -0.102 | 260.36 | 0.495 | -0.000 | 0.996 |
| 80 | 72.02 | -0.554 | 0.006 | -0.111 | 251.59 | 0.540 | 0.000 | 1.088 |
| 90 | 63.77 | -0.595 | 0.006 | -1.186 | 243.36 | 0.582 | 0.001 | 1.177 |

**Table 1** Low Eccentricity of Chief Orbit, $\alpha_{0_i} = 0^\circ$

Additionally, the two impulses are separated by nearly 180° of true anomaly. As $\alpha_{0_f}$ increases, an increase in the magnitudes of the radial and normal components of the velocity impulses is observed, resulting in an increase of the total velocity increment.

Figures 12 and 13 show the projection of the relative motion in the $\theta - h$ plane, for the formation in transit for two different cases with the Chief in the low eccentricity orbit specified above. The first case reconfigures from $\alpha_0 = 0^\circ$ to $\alpha_0 = 90^\circ$, and the second reconfigures the other way round.

*High Eccentricity Reconfiguration*: The reconfiguration from an initial formation characterized by $\rho_i = 10$km to one characterized by $\rho_i = 20$km is studied. Similar to the low eccentricity example, the variation of total impulse required with final phase angle is obtained for two initial phase angles, $\alpha_0 = 0^\circ$ and $\alpha_0 = 90^\circ$. The results are presented in Tables 2 and 3. The tangential component of the velocity impulse is no longer negligible in comparison with the radial and normal components.

| $\alpha_{0_f}$ (deg) | Impulse 1 | | | | Impulse 2 | | | |
|---|---|---|---|---|---|---|---|---|
| | $f_{C_1}$ (deg) | $\Delta\mathbf{v}_1$ (m/s) | | | $f_{C_2}$ (deg) | $\Delta\mathbf{v}_2$ (m/s) | | |
| | | $\Delta v_{1_r}$ | $\Delta v_{1_\theta}$ | $\Delta v_{1_h}$ | | $\Delta v_{2_r}$ | $\Delta v_{2_\theta}$ | $\Delta v_{2_h}$ |
| 0 | 156.17 | 0.102 | -0.240 | -0.260 | 200.42 | 0.021 | 0.140 | -0.171 |
| 10 | 155.71 | 0.130 | -0.268 | -0.310 | 206.08 | -0.004 | 0.086 | -0.036 |
| 20 | 146.32 | 0.135 | -0.246 | -0.462 | 217.78 | -0.006 | 0.041 | 0.039 |
| 30 | 144.58 | 0.091 | -0.172 | -0.568 | 212.81 | 0.012 | 0.063 | 0.167 |
| 40 | 144.26 | 0.053 | -0.108 | -0.665 | 207.23 | 0.019 | 0.065 | 0.286 |
| 50 | 143.52 | 0.013 | -0.038 | -0.770 | 202.97 | 0.025 | 0.060 | 0.388 |
| 60 | 142.65 | -0.033 | 0.042 | -0.865 | 199.67 | 0.037 | 0.054 | 0.480 |
| 70 | 141.77 | -0.087 | 0.131 | -0.942 | 197.07 | 0.055 | 0.049 | 0.564 |
| 80 | 140.96 | -0.146 | 0.225 | -0.995 | 194.96 | 0.078 | 0.046 | 0.640 |
| 90 | 140.20 | -0.206 | 0.321 | -1.017 | 193.21 | 0.104 | 0.041 | 0.705 |

**Table 2** High Eccentricity of Chief Orbit, $\alpha_{0_i} = 0°$

| $\alpha_{0_f}$ (deg) | Impulse 1 | | | | Impulse 2 | | | |
|---|---|---|---|---|---|---|---|---|
| | $f_{C_1}$ (deg) | $\Delta\mathbf{v}_1$ (m/s) | | | $f_{C_2}$ (deg) | $\Delta\mathbf{v}_2$ (m/s) | | |
| | | $\Delta v_{1_r}$ | $\Delta v_{1_\theta}$ | $\Delta v_{1_h}$ | | $\Delta v_{2_r}$ | $\Delta v_{2_\theta}$ | $\Delta v_{2_h}$ |
| 0 | 156.90 | 0.517 | -0.865 | 0.133 | 199.14 | -0.297 | -0.139 | -0.730 |
| 10 | 155.74 | 0.386 | -0.697 | -0.010 | 198.67 | -0.166 | 0.016 | -0.587 |
| 20 | 154.84 | 0.256 | -0.527 | -0.153 | 198.99 | -0.033 | 0.171 | -0.444 |
| 30 | 157.47 | 0.111 | -0.334 | -0.297 | 202.56 | 0.107 | 0.328 | -0.286 |
| 40 | 156.36 | 0.169 | -0.383 | -0.377 | 201.71 | 0.021 | 0.196 | -0.147 |
| 50 | 155.00 | 0.183 | -0.366 | -0.446 | 209.48 | -0.008 | 0.097 | -0.024 |
| 60 | 147.32 | 0.151 | -0.279 | -0.509 | 210.27 | -0.014 | 0.049 | 0.035 |
| 70 | 144.03 | 0.091 | -0.169 | -0.532 | 206.97 | 0.002 | 0.052 | 0.123 |
| 80 | 143.62 | 0.036 | -0.072 | -0.518 | 203.89 | 0.010 | 0.042 | 0.215 |
| 90 | 142.95 | -0.011 | 0.014 | -0.489 | 201.11 | 0.011 | 0.015 | 0.286 |

**Table 3** High Eccentricity of Chief Orbit, $\alpha_{0_i} = 90°$

Figure 11 shows the total impulse required for reconfiguration in the above cases. Unlike the low eccentricity example, no symmetry is observed between the total velocity impulse required for $\alpha_{0_i} = 0°$ and $\alpha_{0_i} = 90°$. It is also observed that the impulses take place almost symmetrically in close proximity of the apogee. Since the velocity of a spacecraft is lowest near apogee, lower velocity increments are required for orbit changes in this region. It is also known from equation (12), that for low eccentricity orbits, inclination changes are most efficiently obtained at the equator, while right ascension changes are most efficiently obtained at zenith or nadir. However, for highly eccentric orbits, the least total velocity impulse

is obtained by a trade-off between the in-plane and out-of-plane impulses. This results in different positions of impulse application, all approximately in the same region ($f_{C_1} \approx 155^\circ$, $f_{C_2} \approx 205^\circ$). For very high eccentricities such as the one considered, eccentricity effects will dominate the fuel requirement.

If the formation had been established at the apogee then the the two impulses can no longer be chosen symmetrically about the apogee without the second impulse occurring almost after one orbit around the Earth. For orbits with high semi-major axes such as the one considered, the time period is almost one day, which results in the two impulses being separated by almost one day.

Figure 14 shows the relative motion of the Deputy under the effect of the two impulses for a reconfiguration from ($\rho = 10\text{km}, \alpha_0 = 0^\circ$) to ($\rho = 20\text{km}, \alpha_0 = 90^\circ$). The impulses required, and where in the orbit they are applied, are given in the last row of Table 2. Figure 15 shows the reconfiguration from ($\rho = 20\text{km}, \alpha_0 = 0^\circ$) to ($\rho = 10\text{km}, \alpha_0 = 90^\circ$).

## Concluding Remarks

A method for accurate propagation of relative motion dynamics of satellites in high eccentricity orbits has been developed. The relative motion is first described on a unit sphere and then transformed into the physical space. Even though the mean orbital elements and secular drift rates are used in the propagation, one can easily transform these into osculating elements or use only the short-period corrections, depending on the accuracy desired. The key feature of the method is the use of true anomaly as the independent variable instead of time. The analytical model is utilized for computing impulsive-thrust reconfiguration

trajectories using numerical optimization. Results are provided for reconfiguration problems for large relative orbits and high eccentricities including the influence of $J_2$.

## Acknowledgements

This research was supported by NASA Grant NAG5-11349 and a grant from the Advanced Technology Program funded by the Texas Board of Higher Education. The authors are grateful to Dr. Dong-Woo Gim for the help he has provided through our discussions with him. This paper is dedicated to Prof. John L. Junkins for his friendship and guidance.

## References

[1] CLOHESSY, W. H., "Terminal Guidance System for Satellite Rendezvous," *Journal of Aerospace Sciences*, Vol. 27, September 1960, pp. 653–658,674.

[2] VADDI, S. S., VADALI, S. R., and ALFRIEND, K. T., "Formation Flying: Accommodating Nonlinearity and Eccentricity Perturbations," *AAS/AIAA Space Flight Mechanics Meeting*, No. AAS 02-184, AAS Publications, San Antonio, Texas, January 2002.

[3] SCHAUB, H. and ALFRIEND, K. T., "$J_2$ Invariant Relative Orbits for Formation Flying," *International Journal of Celestial Mechanics and Dynamical Astronomy*, Vol. 79, 2001, pp. 77–95.

[4] VADALI, S. R., VADDI, S. S., and ALFRIEND, K. T., "A New Concept for Controlling Formation Flying Satellite Constellations," *AAS/AIAA Space Flight Mechanics*

*Meeting*, No. AAS 01-218, AAS Publications, Santa Barbara, California, February 2001.

[5] GIM, D.-W. and ALFRIEND, K. T., "The State Transition Matrix of Relative Motion for the Perturbed Non-Circular Reference Orbit," *AAS/AIAA Space Flight Mechanics Meeting*, No. AAS 01-222, AAS Publications, Santa Barbara, California, February 2001.

[6] SCHAUB, H., "Incorporating Secular Drifts into the Orbit Element Difference Description of Relative Orbits," *AAS/AIAA Space Flight Mechanics Meeting*, No. AAS 03-115, AAS Publications, Ponce, Puerto Rico, February 2003.

[7] SABOL, C., MCLAUGHLIN, C. A., and LUU, K. K., "Meet the Cluster Orbits With Perturbations of Keplerian Elements (COWPOKE) Equations," *AAS/AIAA Space Flight Mechanics Meeting*, No. AAS 03-138, AAS Publications, Ponce, Puerto Rico, February 2003.

[8] VADALI, S. R., "An Analytical Solution for Relative Motion of Satellites," *DCSSS Conference*, Cranfield University, Cranfield, UK, July 2002.

[9] JUNKINS, J. L. and TURNER, J. D., *Optimal Spacecraft Rotational Maneuvers*, Elsevier, Amsterdam, The Netherlands, 1986.

[10] BATTIN, R. H., *An Introduction to the Mathematics and Methods of Astrodynamics*, AIAA Education Series, Reston, Virginia, revised ed., 1999.

[11] VADDI, S. S., ALFRIEND, K. T., and VADALI, S. R., "Sub-Optimal Formation Establishment and Reconfiguration Using Impulsive Control," *AAS/AIAA Astrody-*

*namics Specialist Conference*, No. AAS 03-590, AAS Publications, Big Sky, Montana, August 2003.

[12] BROUWER, D., "Solution of the Problem of Artificial Satellite Theory Without Drag," *The Astronomical Journal*, Vol. 64, November 1959, pp. 378–397.

[13] KOZAI, Y., "The Motion of a Close Earth Satellite," *The Astronomical Journal*, Vol. 64, November 1959, pp. 367–377.

[14] VALLADO, D. A., *Fundamentals of Astrodynamics and Applications*, Microcosm Press, El Segundo, California, 2nd ed., 2001.

[15] VADDI, S. S., *Modeling and Control of Satellite Formations*, Ph.D. thesis, Texas A&M University, College Station, Texas, 2003.

[16] GILL, P. E., MURRAY, W., and SAUNDERS, M. A., *Users Guide for SNOPT Version 6, A FORTRAN Package for Large-Scale Nonlinear Programming*, Department of Mathematics, UC San Diego/Systems Optimization Laboratory, Stanford University, La Jolla, CA/Stanford, CA, December 2002.

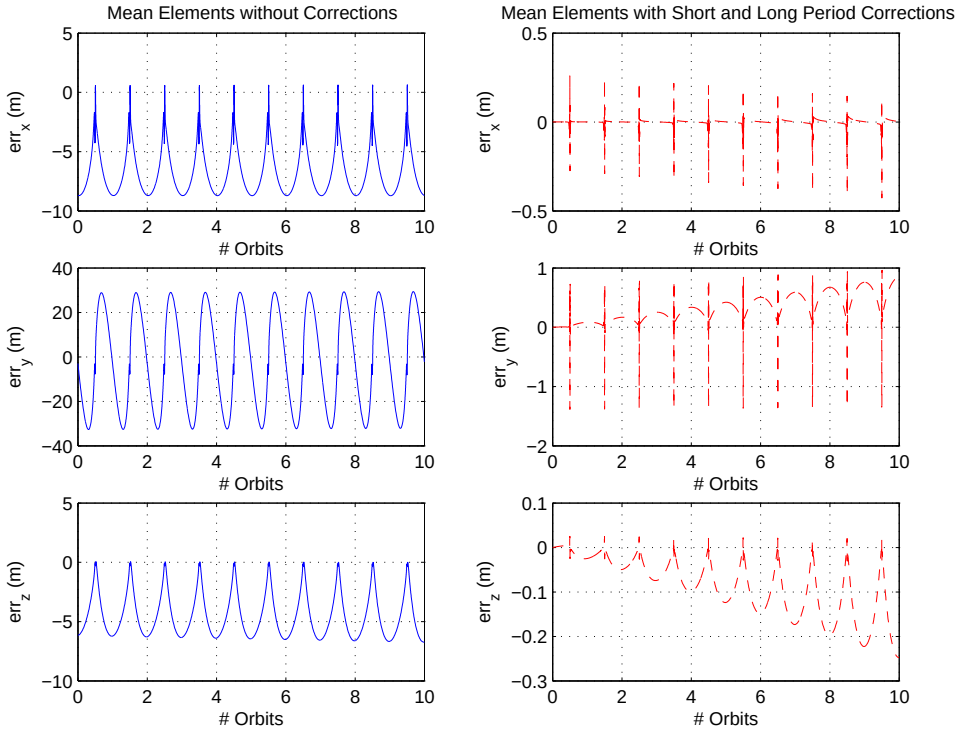


**Figure 2** Errors for $\rho = 20\text{km}$, $\alpha_0 = 0°$

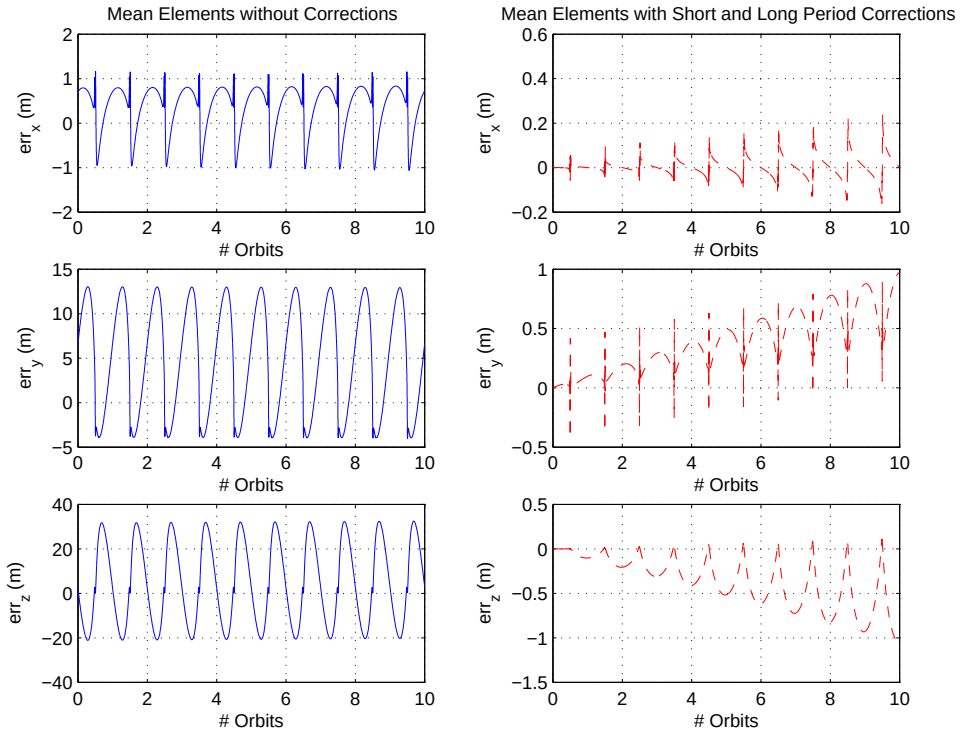


**Figure 3** Errors for $\rho = 20\text{km}$, $\alpha_0 = 90°$

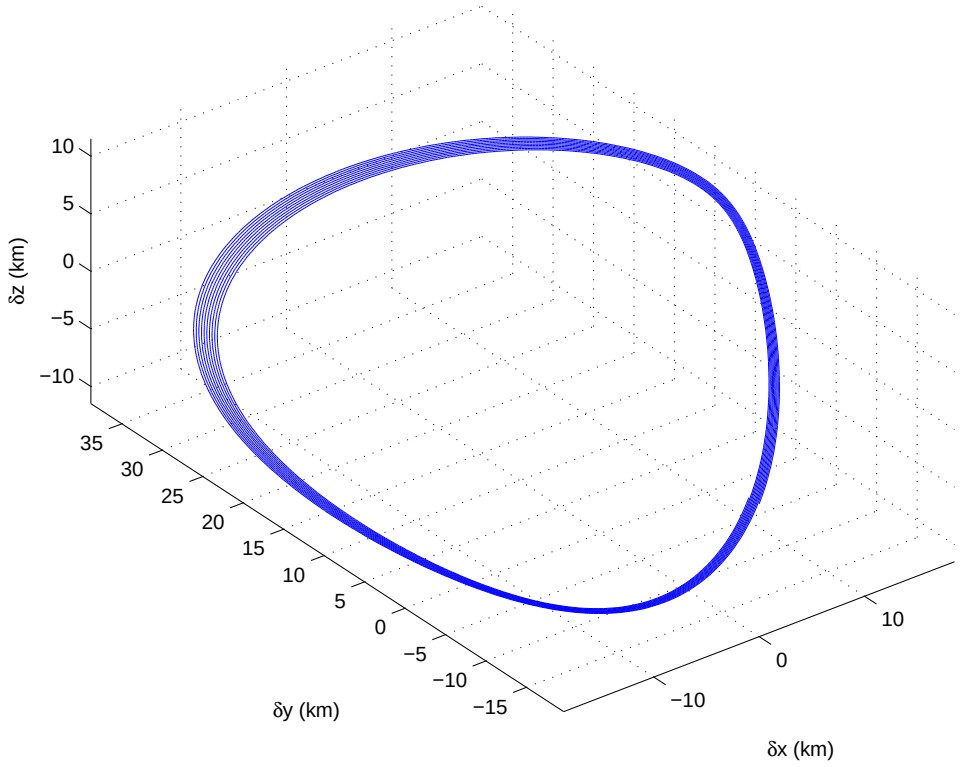


**Figure 4** Relative Orbit Using $\rho = 20\text{km}$, $\alpha_0 = 0°$

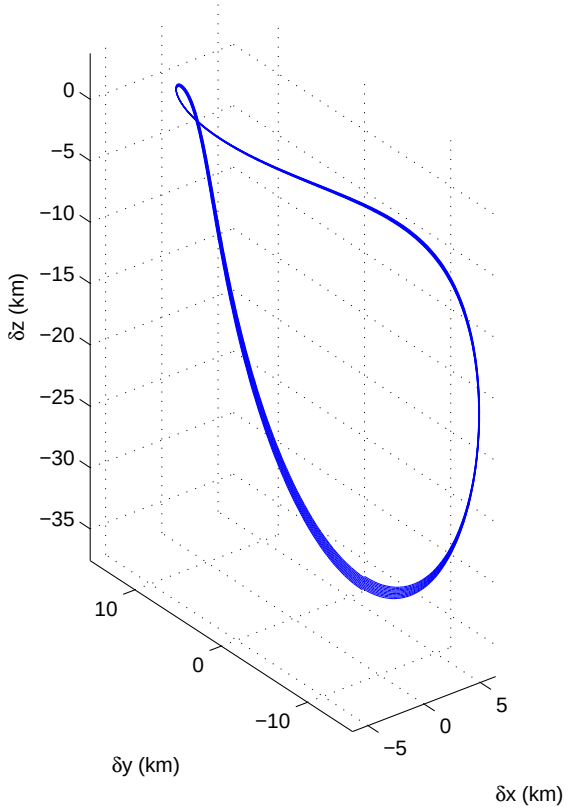


**Figure 5** Relative Orbit Using $\rho = 20\text{km}$, $\alpha_0 = 90°$

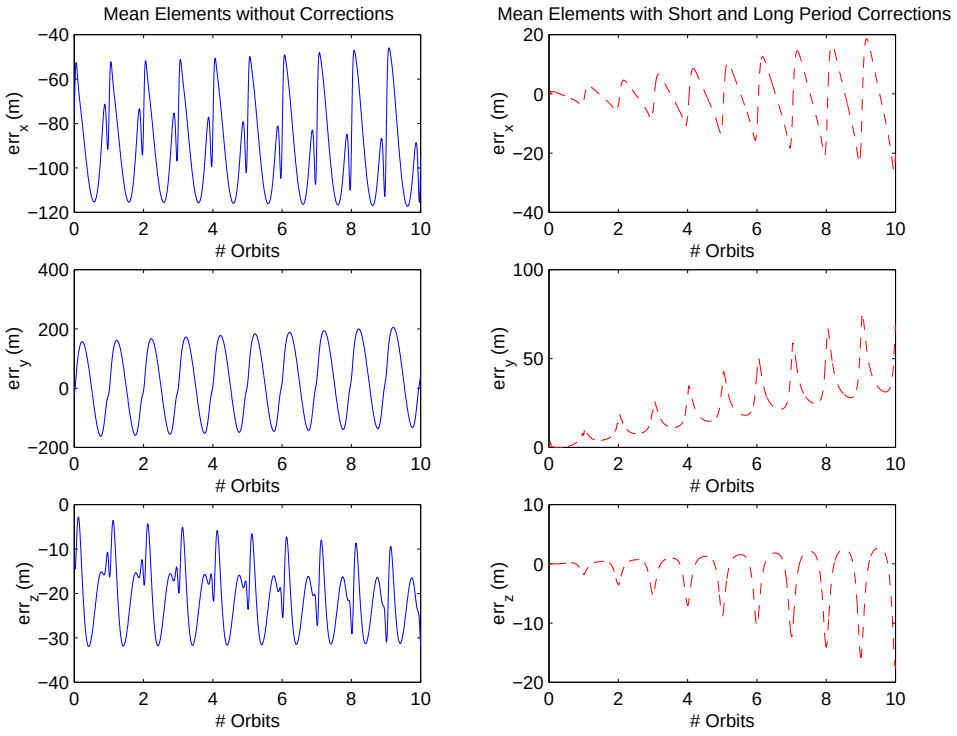


**Figure 6** Errors for $\rho = 100$km, $\alpha_0 = 0°$, Formation Established at Perigee

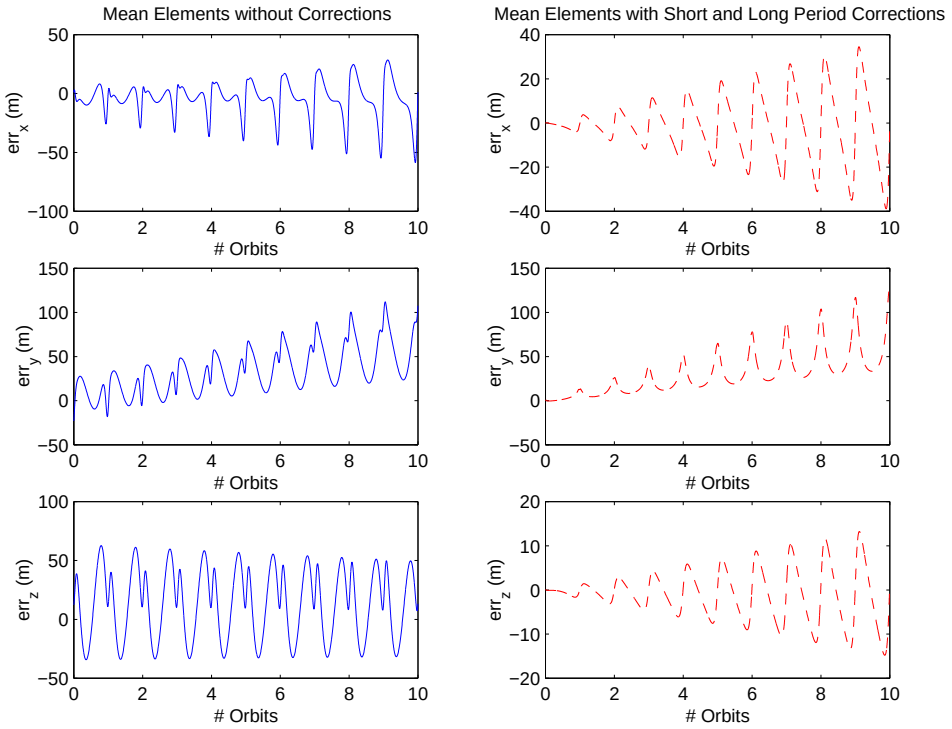


**Figure 7** Errors for $\rho = 100$km, $\alpha_0 = 90°$, Formation Established at Perigee

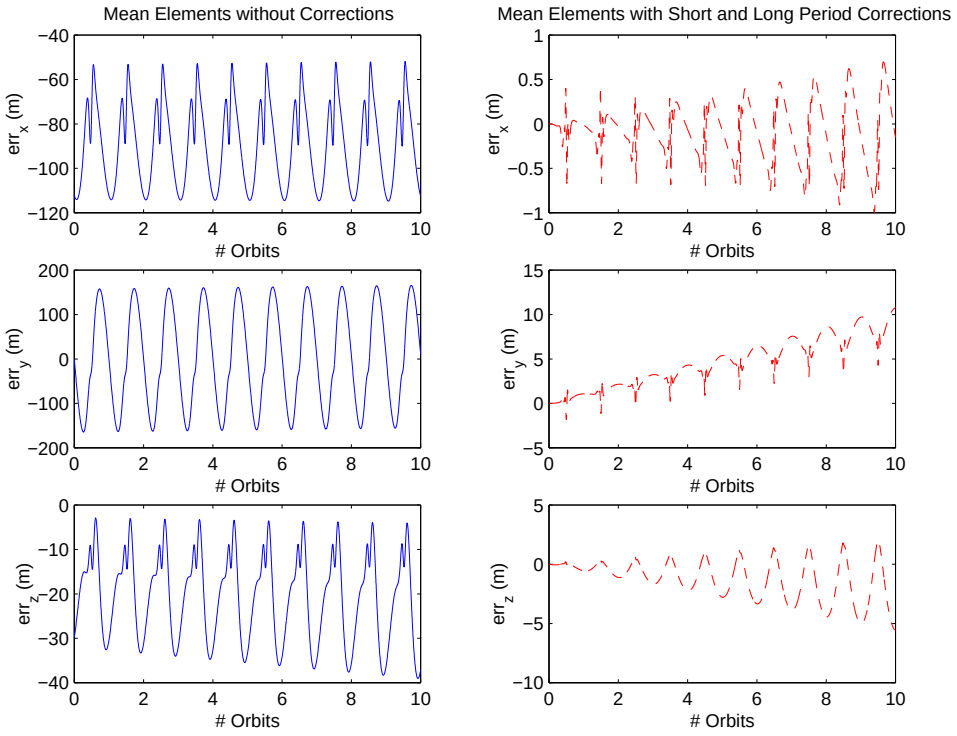


**Figure 8** Errors for $\rho = 100$km, $\alpha_0 = 0°$, Formation Established at Apogee

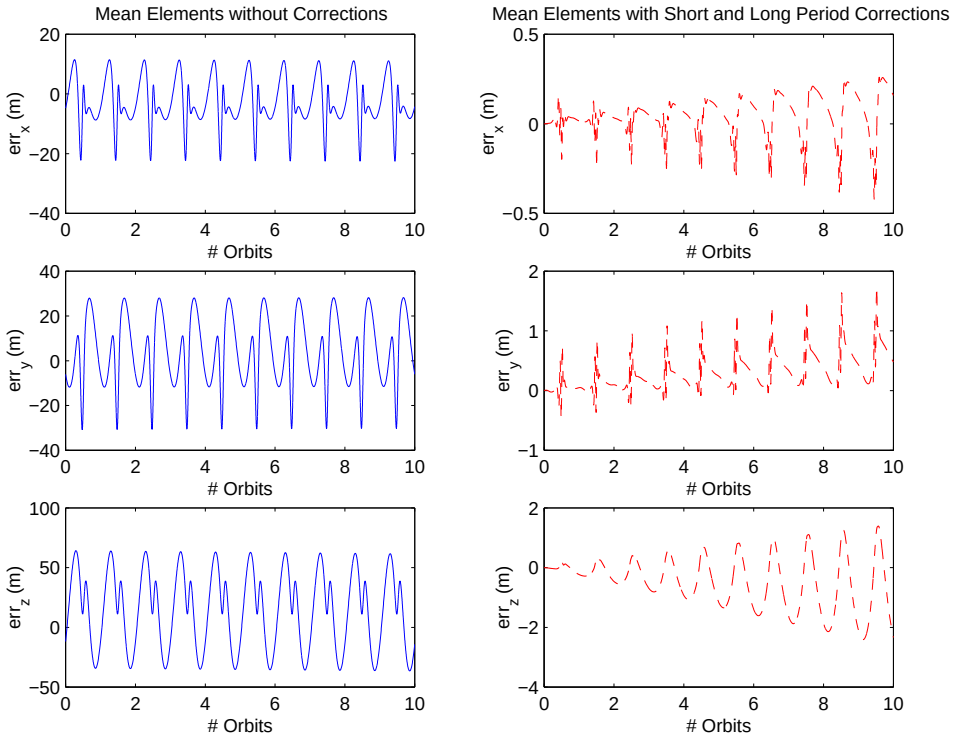


**Figure 9** Errors for $\rho = 100$km, $\alpha_0 = 90°$, Formation Established at Apogee

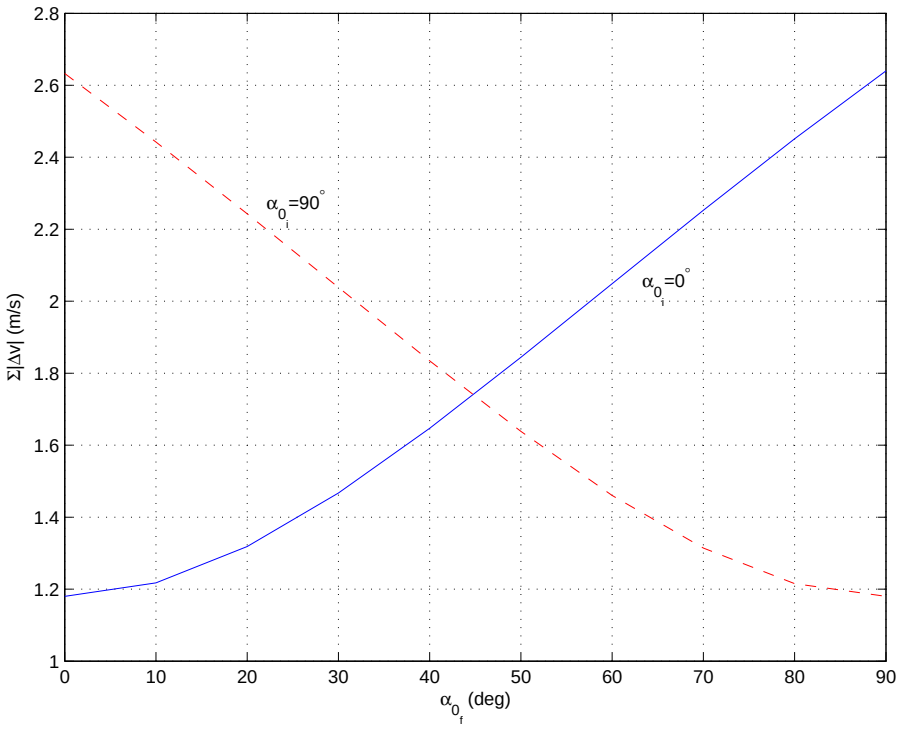


**Figure 10** Total Cost for Reconfiguring Orbit (Low Eccentricity of Chief), for $\alpha_{0_i} = 0°$ and $\alpha_{0_i} = 90°$

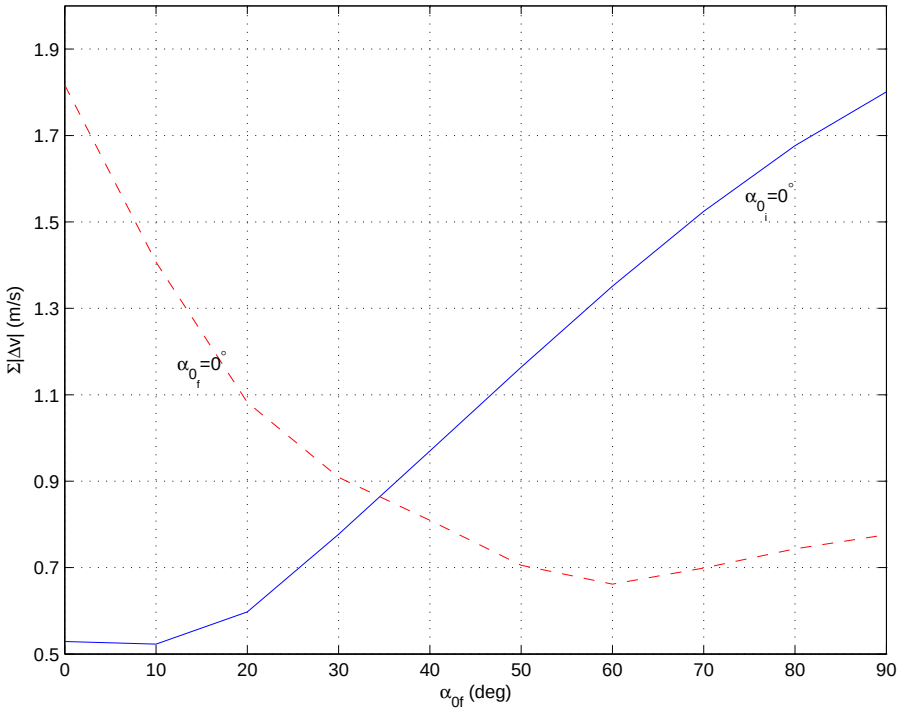


**Figure 11** Total Cost for Reconfiguring Orbit, (High Eccentricity of Chief) for $\alpha_{0_i} = 0°$ and $\alpha_{0_i} = 90°$

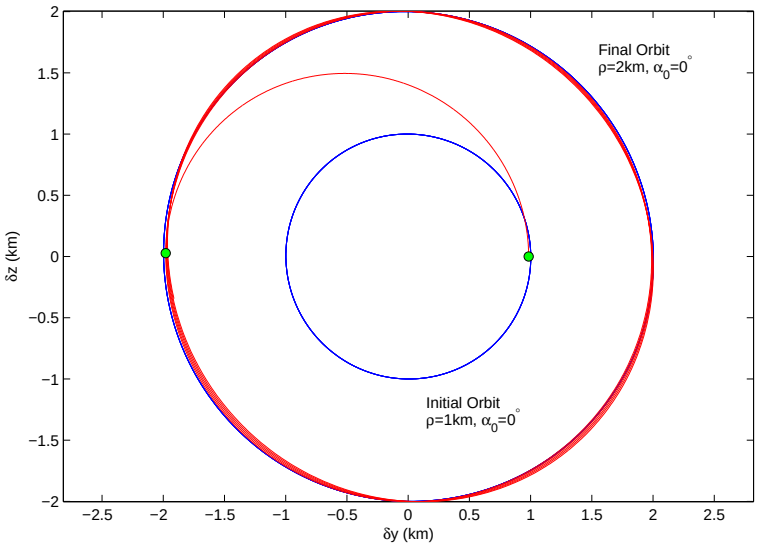


**Figure 12** Relative Orbit Reconfiguration with $J_2$, from $(\rho = 1\text{km}, \alpha_0 = 0°)$ to $(\rho = 2\text{km}, \alpha_0 = 0°)$

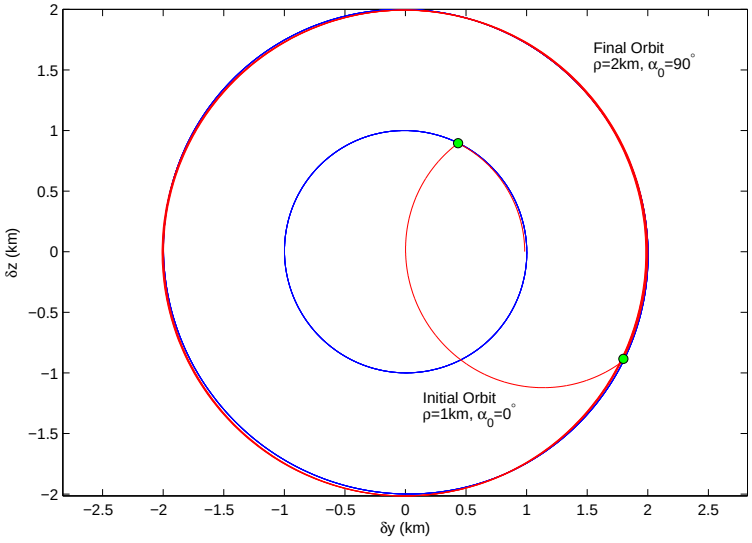


**Figure 13** Relative Orbit Reconfiguration with $J_2$, from $(\rho = 1\text{km}, \alpha_0 = 0°)$ to $(\rho = 2\text{km}, \alpha_0 = 90°)$

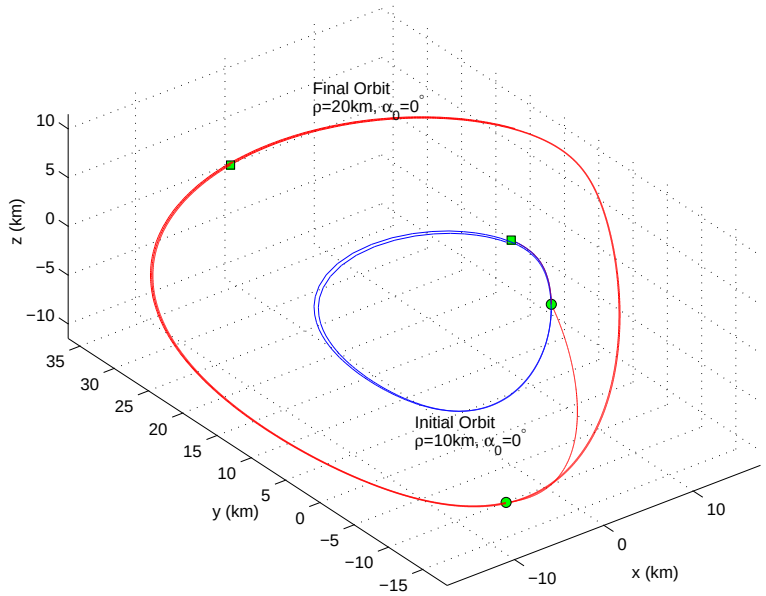


**Figure 14** Relative Orbit Reconfiguration with $J_2$, from $(\rho = 10\text{km}, \alpha_0 = 0°)$ to $(\rho = 20\text{km}, \alpha_0 = 0°)$, High Eccentricity Reference Orbit

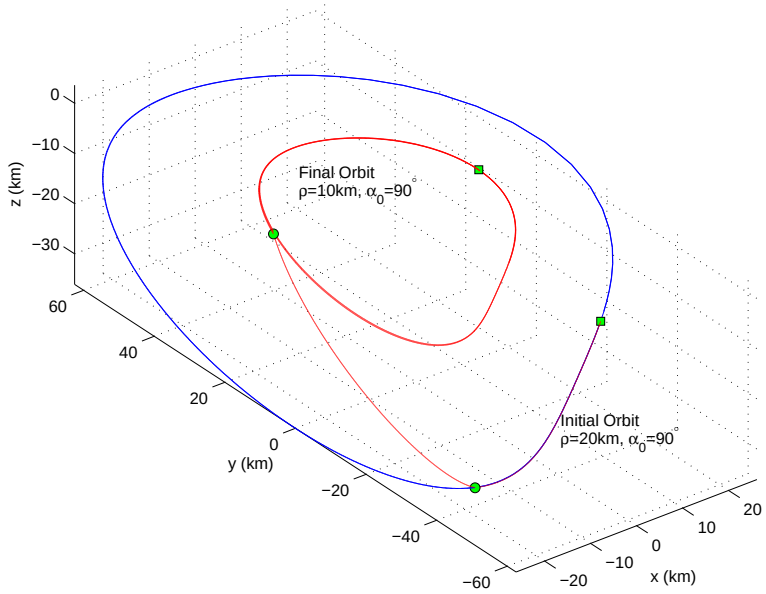


**Figure 15** Relative Orbit Reconfiguration with $J_2$, from $(\rho = 20\text{km}, \alpha_0 = 90°)$ to $(\rho = 10\text{km}, \alpha_0 = 90°)$, High Eccentricity Reference Orbit